

# Continuum Coupling and Single-Nucleon Overlap Integrals

N. Michel,<sup>a,b,c</sup> W. Nazarewicz,<sup>a,b,d</sup> and M. Płoszajczak<sup>e</sup>

<sup>a</sup>*Department of Physics and Astronomy, University of Tennessee, Knoxville, Tennessee 37996, U.S.A.*

<sup>b</sup>*Physics Division, Oak Ridge National Laboratory, Oak Ridge, Tennessee 37831, U.S.A.*

<sup>c</sup>*Department of Physics, Graduate School of Science, Kyoto University Kitashirakawa, 606-8502, Kyoto, Japan*

<sup>d</sup>*Institute of Theoretical Physics, University of Warsaw, ul. Hoża 69, 00-681 Warsaw, Poland*

<sup>e</sup>*Grand Accélérateur National d'Ions Lourds (GANIL), CEA/DSM - CNRS/IN2P3, BP 55027, F-14076 Caen Cedex, France*

---

## Abstract

The presence of a particle continuum, both of a resonant and non-resonant character, can significantly impact spectroscopic properties of weakly bound nuclei and excited nuclear states close to, and above, the particle emission threshold. In the framework of the continuum shell model in the complex momentum-plane, the so-called Gamow Shell Model, we discuss salient effects of the continuum coupling on the one-neutron overlap integrals and the associated spectroscopic factors in neutron-rich helium and oxygen nuclei. In particular, we demonstrate a characteristic near-threshold energy dependence of the spectroscopic factors for different  $\ell$ -waves. We show also that the realistic radial overlap functions, which are needed for the description of transfer reactions, can be generated by single-particle wave functions of the appropriately chosen complex potential.

*Key words:* Shell model, Continuum, Gamow shell model, Spectroscopic factors, Overlap integrals, Exotic Nuclei

*PACS:* 21.60.Cs, 25.60.Je, 21.10.Jx, 25.70.Ef, 03.65.Nk

---

## 1 Introduction

Today, much interest in various fields of physics is devoted to the study of small, open quantum systems (OQS), whose properties are profoundly affected

by the environment, i.e., continuum of decay channels. Although every finite fermion system has its own characteristic features, resonance phenomena are generic; they are great interdisciplinary unifiers. Many of these phenomena have been originally studied in nuclear reactions, and now they are explored in molecules in strong external fields, quantum dots and wires, and other solid state micro-devices, crystals in laser fields, and microwave cavities.

In the field of nuclear physics, a growing interest in the theory of OQSs is associated with experimental efforts in producing weakly bound and unbound nuclei close to the particle drip lines, and studying structures and reactions with those exotic systems. In this context, the major challenge for nuclear theory is to develop theories that would allow to understand properties of those exotic physical systems possessing new and different properties [1,2,3]. To this end, a unification of structure and reaction aspects of weakly bound or unbound nuclei, based on the OQS formalism, is called for.

The nuclear shell model (SM) is the cornerstone of our understanding of nuclei. In its standard realization [2,4], the SM assumes that the many-nucleon system is perfectly isolated from an external environment of scattering states and decay channels. The validity of such a closed quantum system (CQS) framework is sometimes justified by relatively high one-particle (neutron or proton) separation energies in nuclei close to the valley of beta stability. However, weakly bound or unbound nuclear states cannot be treated in a CQS formalism. A consistent description of the interplay between scattering states, resonances, and bound states in the many-body wave function requires an OQS formulation (see Ref. [3] and references quoted therein). Properties of unbound states lying above the particle (or cluster) threshold directly impact the continuum structure. Coupling to the particle continuum is also important for weakly bound states, such as halos. A classic example of a threshold effect is the Thomas-Ehrman shift [5], which manifests itself in the striking asymmetry in the energy spectra between mirror nuclei. (See Ref. [6] for more discussion and examples related to this point.)

In this work, we investigate the impact of the non-resonant continuum on single-nucleon overlap integrals and spectroscopic factors in weakly bound and unbound nuclear states. Our paper is organized as follows. The model used is the SM in the complex momentum-plane, the so-called Gamow Shell Model (GSM) [7,8,9], which is briefly presented in Sec. 2. Section 3 describes the concrete realization of the GSM employed in this work, i.e., interactions used and the GSM model space, as well as the approximate schemes that have been introduced to illuminate specific physics points. The discussion of spectroscopic factors and overlap integrals is contained in Sec. 4. We show that the realistic radial overlap functions, which are needed for the description of transfer reactions, can be generated by single-particle wave functions of the appropriately chosen *complex average potential* reproducing the complex  $Q$ -

value of the studied reaction or decay. Furthermore, we demonstrate that the scattering continuum is of crucial importance for the spectroscopic factors in the vicinity of the particle emission threshold. This problem has been discussed recently in our work [10] for the  $\ell = 1$  neutron waves. Here, we extend this discussion to  $\ell = 2$  and also compare the spectroscopic factors in GSM with those calculated in the pole approximation to see the influence of non-resonant continuum. As an illustrative example in these studies, we choose the case of *model* two-neutron systems outside the inert core:  ${}^6\text{He}$  and  ${}^{18}\text{O}$ . Our aim is not to fit the actual experimental data, but rather to illustrate generic effects. Finally, the conclusions of this work are summarized in Sec. 5.

## 2 Gamow Shell Model

As the Gamow Shell Model has been described in detail in a number of publications, only rudimentary information is provided here. In the roots of GSM lies the Berggren one-body completeness relation [11,12] that provides the mathematical foundation for unifying bound and unbound states. The Berggren ensemble consists of bound, resonant, and scattering s.p. wave functions, generated by a finite-depth potential  $V(r)$ , either real or complex. The wave functions are regular solutions of the s.p. Schrödinger equation,

$$u_{\mathcal{B}}''(r) = \left[ \frac{\ell(\ell+1)}{r^2} + \frac{2m}{\hbar^2}V(r) - k^2 \right] u_{\mathcal{B}}(r), \quad (1)$$

that obey outgoing or scattering boundary conditions:

$$u_{\mathcal{B}}(r)_{r \rightarrow +\infty} = C_+ H_{\ell}^+(kr) + C_- H_{\ell}^-(kr), \quad (2)$$

where  $k = \sqrt{2mE}/\hbar$  is the complex wave number. For the resonant states,  $C_- = 0$  (outgoing boundary condition). In this paper, as we consider only valence neutrons,  $H_{\ell}^{\pm}$  is a Hankel function. Normalization constants  $C_+$  and  $C_-$  are determined from the condition that the radial wave functions  $u(r)$  are normalized to unity (for resonant states) or to the Dirac delta (for scattering states).

For a given partial wave  $(\ell, j)$ , the scattering states are distributed along the contour  $L_+^{\ell_j}$  in the complex momentum plane. The set  $|u_{\mathcal{B}}\rangle$  of all bound and resonant states enclosed between  $L_+^{\ell_j}$  and the real  $k$ -axis, and scattering states is complete [11]:

$$\sum_{\mathcal{B}}^{\int} |u_{\mathcal{B}}\rangle \langle \widetilde{u}_{\mathcal{B}}| = 1. \quad (3)$$

The Gamow (and Berggren) states are vectors in the rigged Hilbert space (or Gelfand triplet) [13,14,15,16]. Consequently, in the above, the tilde symbol signifies that the complex conjugation arising in the dual space affects only the angular part and leaves the radial wave function unchanged [11,12]. The Berggren states are normalized using the squared radial wave function and not the modulus of the squared radial wave function. In the standard SM treatment, the latter normalization is used.

In numerical applications, the integral over scattering states along  $L_+^{\ell_j}$  has to be discretized and the selected scattering states have to be renormalized [7]. This leads to a discrete completeness relation:

$$\sum_{\mathcal{B}=1}^N |u_{\mathcal{B}}\rangle \langle \widetilde{u}_{\mathcal{B}}| \simeq 1 \quad ; \quad |u_{\mathcal{B}}\rangle = \sqrt{\omega_{\mathcal{B}}} |u_{k_{\mathcal{B}}}\rangle, \quad (4)$$

where  $\{k_{\mathcal{B}}, \omega_{\mathcal{B}}\}$  is the set of discretized complex wave numbers and associated weights provided by a Gauss-Legendre quadrature. As discussed in Ref. [17], the Gauss-Legendre integration formula offers an excellent precision at a modest number ( $\sim 30$ ) of discretization points.

The many-body Berggren basis is that of Slater determinants built from s.p. states of Eqs. (2-4):

$$|SD_i\rangle = |u_{i_1} \cdots u_{i_A}\rangle, \quad (5)$$

where the index  $i$  labels the many-body basis, and  $u_{i_j}$  is the  $j$ -th s.p. state occupied in  $|SD_i\rangle$ . The many-body completeness relation is a consequence of Eq. (5); it is obtained by forming all possible many-body Slater determinants:

$$\sum_i |SD_i\rangle \langle \widetilde{SD}_i| \simeq 1. \quad (6)$$

The equality in Eq. (6) is not exact due to the discretization of the one-body completeness relation.

In the Berggren representation, the SM Hamiltonian matrix  $H$  becomes complex symmetric. Its complex-energy eigenvectors can be obtained by using the complex Lanczos method [18]. The fundamental difference between GSM and the real-energy SM is that the many-body resonant states of the GSM are embedded in the background of scattering eigenstates, so that one needs a criterion to isolate them. The overlap method introduced in Ref. [7] has proven to be very efficient in this respect. To this end, one diagonalizes  $H$  in the basis spanned on the s.p. resonant states only (the so-called pole approximation);

this yields a zeroth-order approximation  $|\Psi_0\rangle$  for the wave function. The vector  $|\Psi_0\rangle$  has a correct outgoing behavior; it is used as a pivot to generate a Lanczos subspace of the full GSM space. The requested resonant eigenstate of  $H$  is the one which maximizes the overlap  $|\langle\Psi_0|\Psi\rangle|$ . The overlap method has also been employed in the Density Matrix Renormalization Group (DMRG) technique [19] recently generalized to treat the non-hermitian GSM case [20].

The definition of observables in GSM follows directly from the mathematical setting of quantum mechanics in the rigged Hilbert space [13,14,15,16] rather than the usual Hilbert space. A modified definition of the dual space, embodied by the tilde symbol above the bra states in Eqs. (3-6), implies that observables in many-body resonances become complex. In this case, the real part of a matrix element corresponds to the expectation value, and the imaginary part can be interpreted as the uncertainty in the determination of this expectation value due to the possibility of decay of the state during the measuring process [11,16,21]. That is a standard price for replacing the time-dependent description of an unstable system by the quasi-stationary description.

### 3 Gamow Shell Model Implementation

This section contains details pertaining to GSM calculations carried out in this work. It describes the Hamiltonian used, the choice of the active Hilbert space, and the approximations employed. All remaining details of the formalism can be found in Refs. [7,10].

#### 3.1 GSM Hamiltonian

The doubly magic nuclei  ${}^4\text{He}$  and  ${}^{16}\text{O}$  are assumed to be the inert cores in our helium and oxygen calculations, respectively. The GSM Hamiltonian consists of a one-body Woods-Saxon (WS) potential, representing a core-valence interaction, and a two-body residual interaction:

$$H = \sum_i \left[ \frac{p_i^2}{2m} + V_{WS}(r_i) \right] + V_{res}^{(2)}. \quad (7)$$

The WS potential contains the central term and the spin-orbit term:

$$V(r) = -V_{WS} \cdot f(r) - 4 V_{so} (\vec{l} \cdot \vec{s}) \frac{1}{r} \left| \frac{df(r)}{dr} \right|, \quad (8)$$

where  $V_{WS}$  and  $V_{so}$  are the strength constants and

$$f(r) = \left[ 1 + \exp\left(\frac{r - R_0}{d}\right) \right]^{-1} \quad (9)$$

is the WS form-factor characterized by radius  $R_0$  and diffuseness  $d$ . In the helium calculations, we employed the “ ${}^5\text{He}$ ” WS parameter set [7] which reproduces the experimental energies and widths of known s.p. resonances  $3/2_1^-$  and  $1/2_1^-$  in  ${}^5\text{He}$  ( $0p_{3/2}$  and  $0p_{1/2}$  resonant states in our model). In the oxygen case, we used the “ ${}^{17}\text{O}$ ” WS parameter set [7] that reproduces experimental energies and widths of the  $5/2_1^+$  and  $1/2_1^+$  bound states and the  $3/2_1^+$  resonance in  ${}^{17}\text{O}$  (i.e.,  $0d_{5/2}$ ,  $1s_{1/2}$ , and  $0d_{3/2}$  resonant states).

We used a different residual interaction for helium and oxygen isotopes. This choice has been motivated by our previous studies of oxygen, helium, and lithium chains [7,8]. For the heliums, we took the finite-range surface Gaussian interaction (SGI) [8]

$$V_{res}^{(2)} = \sum_{i < j} V_0^{(J)} \cdot \exp\left(-\left[\frac{|\vec{r}_i - \vec{r}_j|}{\mu}\right]^2\right) \cdot \delta(|\vec{r}_i| + |\vec{r}_j| - 2R_0) \quad (10)$$

with the range  $\mu=1\text{ fm}$  and the coupling constants depending on the total angular momentum  $J$  of the neutron pair:  $V_0^{(0)} = -403\text{ MeV fm}^3$ ,  $V_0^{(2)} = -392\text{ MeV fm}^3$ . These constants are fitted to reproduce the ground-state (g.s.) binding energies of  ${}^6\text{He}$  and  ${}^7\text{He}$  in GSM.

For the oxygens, we employed a surface delta interaction (SDI) [8]:

$$V_{res}^{(2)} = \sum_{i < j} V_0 \cdot \delta(\vec{r}_i - \vec{r}_j) \cdot \delta(|\vec{r}_i| - R_0), \quad (11)$$

where the SDI coupling constant  $V_0 = -700\text{ MeV fm}^3$  was fitted to in order to reproduce the two-neutron separation energy of  ${}^{18}\text{O}$ .

### 3.2 GSM Configuration Space

In the helium variant, the valence space consists of the  $p_{3/2}$  and  $p_{1/2}$  neutron partial waves. The  $p_{3/2}$  wave functions include a  $0p_{3/2}$  resonant state and  $p_{3/2}$  non-resonant scattering states along a complex contour enclosing the  $0p_{3/2}$  resonance in the complex  $k$ -plane. For a  $p_{1/2}$  part, we take non-resonant scattering states along the real- $k$  axis (the broad  $0p_{1/2}$  resonant state plays a negligible role in the g.s. wave function of  ${}^6\text{He}$ ). For both contours, the maximal momentum value is  $k_{\max} = 3.27\text{ fm}^{-1}$ . The contours have been discretized

with up to 60 points, and the attained precision on energies and widths is better than 0.1 keV.

In the oxygen case, the valence GSM space for neutrons consists of the  $0d_{5/2}$ ,  $1s_{1/2}$ , and  $0d_{3/2}$  Gamow states and the non-resonant complex  $d_{3/2}$  continuum. The  $0d_{5/2}$  and  $1s_{1/2}$  shells are bound while the  $0d_{3/2}$  state is a narrow resonance. The maximum value for  $k$  on the contour  $L_+^{d_{3/2}}$  is  $k_{\max} = 1.5 \text{ fm}^{-1}$ . The contour has been discretized with 45 points and the resulting precision on energies and widths is  $\sim 0.1 \text{ keV}$ . The real-energy  $d_{5/2}$  and  $s_{1/2}$  contours give rise to a renormalization of the residual interaction coupling constant; hence, they have been neglected [7].

### 3.3 Simplified SM schemes: GSM-p and HO-SM

In order to illuminate certain aspects of GSM results (e.g., non-resonant continuum coupling or configuration mixing), we have introduced two simplified SM schemes: the GSM in the pole approximation (GSM-p) and the harmonic oscillator shell model (HO-SM).

In GSM-p, the scattering components of the Berggren basis are disregarded, and only the resonant states are present in the basis. In particular, they will be the  $0p_{3/2}$  and  $0p_{1/2}$  neutron states for heliums, and  $0d_{5/2}$ ,  $1s_{1/2}$ , and  $0d_{3/2}$  neutron states for oxygens. In this case, the one-body completeness relation (3) is obviously violated. Still, the comparison between full GSM results and GSM-p is instructive as it illustrates the influence of the non-resonant continuum subspace on the GSM results.

For the HO-SM calculation, the radial wave functions of the GSM-p basis are replaced by those of the spherical harmonic oscillator (HO) with the frequency  $\hbar\omega = 41A^{-1/3} \text{ MeV}$ . The real energies of the resonant states define the one-body part of the HO-SM Hamiltonian. The HO-SM scheme is intended to illustrate the “standard” CQS SM calculations in which only bound valence shells are considered in the s.p. basis.

## 4 One-nucleon overlap integrals and spectroscopic factors in GSM

### 4.1 Definitions

Single-nucleon overlap integrals and the associated spectroscopic factors are basic ingredients of the theory of direct reactions (single-nucleon transfer, nu-

neutron knockout, elastic break-up) [22,23,24,25]. Experimentally, spectroscopic factors can be deduced from measured cross sections; they are useful measures of the configuration mixing in the many-body wave function. The associated reaction-theoretical analysis often reveals model- and probe-dependence [26,27,28] raising concerns about the accuracy of experimental determination of spectroscopic factors. In our study we discuss the uncertainty in determining spectroscopic factors due to the two assumptions commonly used in the standard SM studies, namely (i) that a nucleon is transferred to/from a specific s.p. orbit (corresponding to an observed s.p. state), and (ii) that the transfer to/from the continuum of non-resonant scattering states can be disregarded. This discussion complements our recent work [10] whose focus was on threshold anomalies and channel coupling.

The one-nucleon radial overlap integral is discussed in the usual way [23,24,25]:

$$u_{\ell j}(r) = \langle \Psi_A^{J_A}(\vec{r}_1, \dots, \vec{r}_A = \vec{r}) | [ |\Psi_{A-1}^{J_{A-1}}(\vec{r}_1, \dots, \vec{r}_{A-1}) \rangle \otimes |\ell, j \rangle ]^{J_A} \rangle, \quad (12)$$

where  $|\Psi_A^{J_A}\rangle$  and  $|\Psi_{A-1}^{J_{A-1}}\rangle$  are wave functions of nuclei  $A$  and  $A-1$ , respectively, and angular and spin coordinates (represented by  $|\ell, j\rangle$ ) are integrated out so that  $u_{\ell j}$  depends only on  $r = |\vec{r}|$ . The spectroscopic factor is given by the real part of the norm  $S^2$  of the overlap integral. Using a decomposition of the s.p.  $(\ell, j)$  channel in the complete Berggren basis, one obtains GSM expressions for the overlap integral and  $S^2$ :

$$u_{\ell j}(r) = \sum_{\mathcal{B}} \langle \widetilde{\Psi}_A^{J_A} | a_{\ell j}^+(\mathcal{B}) | \Psi_{A-1}^{J_{A-1}} \rangle \langle r \ell j | u_{\mathcal{B}} \rangle \quad (13)$$

$$S^2 \equiv \int u_{\ell j}^2(r) dr = \sum_{\mathcal{B}} \langle \widetilde{\Psi}_A^{J_A} | a_{\ell j}^+(\mathcal{B}) | \Psi_{A-1}^{J_{A-1}} \rangle^2 \quad (14)$$

where  $a_{\ell j}^+(\mathcal{B})$  is a creation operator associated with a s.p. basis state  $|u_{\mathcal{B}}\rangle$ . We wish to emphasize that since Eqs. (13,14) involve summation over all discrete Gamow states and integration over all scattering states along the contour  $L_+^{\ell j}$ , the final result is independent of the s.p. basis assumed (see also Ref. [29] where a model-independent spectroscopic factor experimental extraction procedure is proposed). This is in contrast to the standard SM treatment of spectroscopic factors where model-dependence enters through the specific choice of a s.p. state  $|n\ell j\rangle$  [31], with Eq. (14) reducing to a single matrix element  $|\langle \widetilde{\Psi}_A^{J_A} | a_{n\ell j}^+ | \Psi_{A-1}^{J_{A-1}} \rangle|^2$ .

Spectroscopic factors are often extracted from measured transfer reaction cross sections. (In the context of the following discussion, it is worth noting that while the reaction cross sections are measurable quantities, the spectroscopic factors are purely theoretical concepts. First, they are deduced from experiment in



a model-dependent way. Second, occupation numbers deduced from spectroscopic factors are not observables per se [30].) In the CQS SM framework, the transfer total cross section is given by [32,24,25]:

$$\sigma = \sum_{n\ell jm} S_{n\ell jm} \sigma_{s.p.}^{n\ell jm}, \quad (15)$$

where  $S_{n\ell jm}$  is the spectroscopic factor associated with the  $|n\ell jm\rangle$  s.p. state, and  $\sigma_{s.p.}^{n\ell jm}$  a s.p. cross section containing all the kinetic dependence related to the transfer of the nucleon of the projectile to the shell model state. While Eq. (15) is, in principle, exact for bound s.p. states, as one sums over all quantum numbers  $n\ell jm$ , the commonly used approximation is to take only one radial quantum number  $n$  for each  $\ell jm$  in the sum of Eq. (15), i.e., one assumes that the nucleon is transferred to/from an orbit with a specific radial quantum number. Hence, the resulting value of spectroscopic factor becomes spuriously basis-dependent. We shall show in the following that this can lead to sizeable errors if the states  $|\Psi_A^{JA}\rangle$  or  $|\Psi_{A-1}^{JA-1}\rangle$  are loosely bound.

Obviously, the factorization (15) does not apply to many-body states which cannot be described in the CQS formalism. Firstly, in the OQS formalism the sum in Eq. (15) is not limited to discrete states  $|n\ell jm\rangle$  only. The appearance of the cusp at the channel threshold both in the reaction cross-section and in the real part of the GSM spectroscopic factor suggests an expression:

$$\sigma = \sum_{\ell j} \text{Re}(S_{n\ell j}) \sigma_{s.p.}^{\ell j}, \quad (16)$$

as the relation between the observable reaction cross-section and the real part of the spectroscopic amplitude  $S \equiv S_{n\ell j}$  (cf (14)) calculated in GSM. Secondly, as stated earlier, observables involving unbound states are complex in GSM. It was conjectured by Berggren [11] and later by Gyarmati *et al.* [33] that the real part of a matrix element corresponds to the expectation value. Based on scattering theory, Berggren showed [34] that the real part of the complex cross section for populating a resonance is equal to the energy integral of the in-elastic continuum cross section across the resonance peak. The imaginary part of the cross section can be identified with the strength of the resonance-background interference. This conclusion was later generalized to hold for any observable operator involving resonant states. In this work, we follow Berggren's interpretation and associate an imaginary part of a matrix element (e.g., spectroscopic factors or radial overlap function) with the uncertainty in the determination of the real part of this matrix element.

For weakly bound or unbound nuclei, the transfer reaction cross section is changed by couplings to the non-resonant continuum which modify both the effective interaction among valence particles and the configuration mixing. This

change in the cross section has a regular component having a smooth dependence on the distance from the particle-emission threshold, and an anomalous component which results in the Wigner-cusp phenomenon [35]. Other quantities, such as the strength function [36,37], the continuum-coupling correction to the CQS eigenvalue [38], or the overlap integral [10] are modified in a similar way. These two components can be seen by comparing full GSM results with equivalent SM results (here: the HO-SM approximation).

Generic features of wave functions in the vicinity of the reaction threshold (the particle-emission threshold) are responsible for the anomalous component. Wigner was first to notice it as the characteristic behavior of scattering and reaction cross-sections [35], often referred to as the Wigner threshold law or the Wigner-cusp phenomenon. A quantitative explanation of this behavior of cross sections was given later [39,40,41,42,43,44]. Wigner threshold law tells that in the vicinity of particle-emission thresholds the reaction cross section has a universal shape depending on the charge and the orbital angular momentum of the scattered particle. In particular, the reaction cross section for neutron scattering near the neutron emission threshold shows a characteristic cusp dependence on the orbital momentum of a scattered neutron. This salient  $\ell$ -dependent anomalous behavior (cusp) is absent for charged scattered particles.

Contrary to the universality of the cusp, its magnitude is not a generic feature of OQs and cannot be found from general principles. Also the ratio between regular and anomalous components in the near-threshold behavior of reaction cross-sections, strength functions, radial overlap integrals, spectroscopic factors, or continuum-coupling correction to CQS eigenvalues is the specific property of each considered OQS and its Hamiltonian.

The modification of the cross section in one channel manifests itself due to the unitarity of the scattering matrix in other open channels. This coupling effect has been studied theoretically [40,41,42,43,45,36,10] and experimentally [46,47,48,49] in connection with the Wigner threshold anomaly. The channel-channel continuum coupling influences both the anomalous and regular cross-section components. Similar multi-channel threshold effects are expected to show up in various observables which depend on occupation probabilities of s.p. shells and the configuration mixing involving continuum states.

It was shown in Ref. [10] that once a given nuclear Hamiltonian is chosen, quantities such as the spectroscopic factors, defined in GSM through the norm of the overlap integral, and their behavior close to particle-emission thresholds are defined uniquely in terms of the exact many-body GSM solutions. Below, we shall demonstrate that the threshold variations due to the continuum coupling can be of a comparable size to those generated by the long-range correlations and the coupling to high-momentum states reached by short-range and tensor components of the nucleon-nucleon interaction [50]. Hence, the states

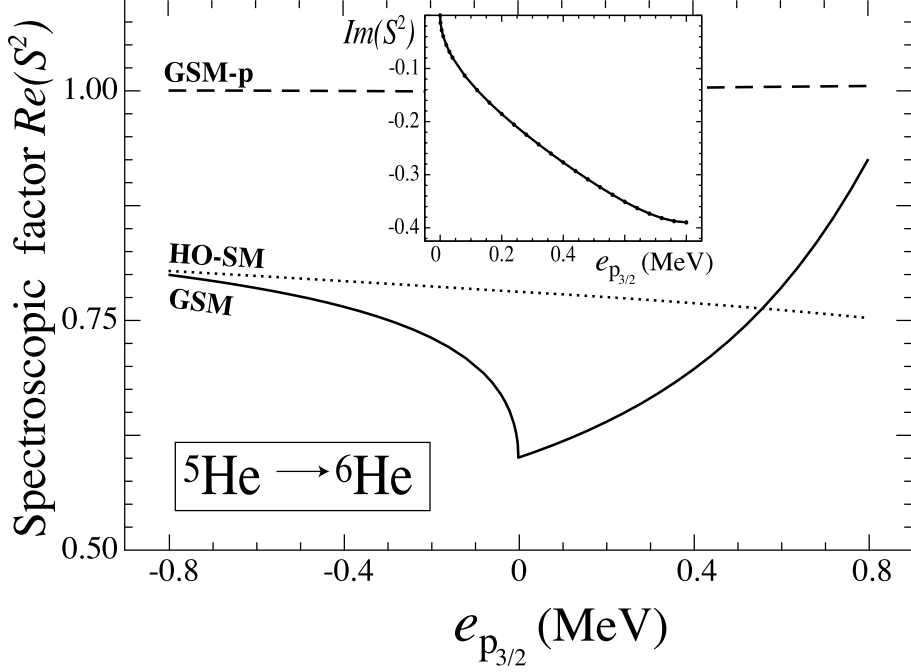


Fig. 1. The real part of the overlap  $\langle {}^6\text{He}(\text{g.s.}) | [{}^5\text{He}(\text{g.s.}) \otimes p_{3/2}]^{0+} \rangle^2$  as a function of the energy of the  $0p_{3/2}$  resonant state.  ${}^6\text{He}$  is always bound. The solid line (GSM) shows the full GSM result. The dotted line (HO-SM) corresponds to the SM calculation in the oscillator basis of  $0p_{3/2}, 0p_{1/2}$ . The dashed line (GSM-p) shows the GSM result in the pole approximation. The imaginary part of  $S^2$  is given in the inset. In order to better illustrate the effect of configuration mixing,  $S^2$  has been normalized to 1 in the limit of vanishing residual interaction.

of *open* and *closed* quantum systems may have not only different asymptotic behavior but also different shell model structure. In that sense, loosely bound or unbound states form a different class of correlated quantum many-body systems than those found in well-bound nuclear states.

#### 4.2 The ${}^5\text{He}+n \rightarrow {}^6\text{He}$ case

We first consider the g.s. spectroscopic factor of  ${}^6\text{He}$  corresponding to the channel  $[{}^5\text{He}(\text{g.s.}) \otimes p_{3/2}]^{0+}$ . In order to investigate the effect of the continuum coupling, the depth of the WS potential is varied so that the energy  $e_{p_{3/2}}$  of the  $0p_{3/2}$  s.p. state (the lowest  $p_{3/2}$  pole of the  $S$ -matrix) changes its character from bound to unbound. In our model space, the energy  $e_{p_{3/2}}$  is both the g.s. energy of  ${}^5\text{He}$  and (negative of) the one-neutron (1n) separation energy  $S_{1n}$  of  ${}^5\text{He}$ .

The calculated spectroscopic factor  $[{}^5\text{He}(\text{g.s.}) \otimes p_{3/2}]^{0+}$  in  ${}^6\text{He}(\text{g.s.})$  is shown in Fig. 1 as a function of the real energy  $e_{p_{3/2}}$  of the  $0p_{3/2}$  pole. In the range of  $e_{p_{3/2}}$  values shown in Fig. 1,  ${}^6\text{He}$  is bound ( $S_{1n}({}^6\text{He}) > 0$ ). The spectroscopic

factor strongly depends on the position of the pole: for  $e_{p_{3/2}} < 0$  ( $S_{1n}({}^5\text{He}) > 0$ ) it decreases with  $e_{p_{3/2}}$  while it increases for  $e_{p_{3/2}} > 0$  ( $S_{1n}({}^5\text{He}) < 0$ ). At the 1n-emission threshold in  ${}^5\text{He}$  ( $e_{p_{3/2}} = 0$ ), spectroscopic factor exhibits a cusp. At this point, the derivative of spectroscopic factor becomes discontinuous and the coupling matrix element between the resonant  $0p_{3/2}$  state and the non-resonant continuum reaches its maximum [38].

As discussed in Ref. [10], the dependence of spectroscopic factor on  $e_{p_{3/2}}$  around  $e_{0p_{3/2}} = 0$  (where the spectroscopic factor exhibits a cusp due to a coupling with the  ${}^4\text{He}+n+n$  channel) follows the threshold behavior of the reaction cross section [35]. Specifically, the anomalous component of spectroscopic factor *below* the 1n threshold in  ${}^5\text{He}$  behaves as  $(-e_{\ell j})^{\ell-1/2}$ . *Above* the threshold, the spectroscopic factor is complex; the real part behaves as  $(e_{\ell j})^{\ell+1/2}$  while the imaginary part, associated with the decaying nature of  ${}^5\text{He}$ , varies as  $(e_{\ell j})^{\ell-1/2}$ .

To assess the role of the continuum, both resonant and non-resonant, the GSM results are compared in Fig. 1 with the HO-SM and GSM-p calculations. In contrast to GSM, spectroscopic factors in HO-SM and GSM-p vary little in the energy range considered and no threshold effect is seen. It is interesting to note that in the limit of an appreciable binding, the  $0p_{3/2}$  wave function is fairly well localized, the importance of the continuum coupling is diminished, and the HO-SM result approaches the GSM limit. For  $e_{p_{3/2}} > 0$ , GSM results are in strong disagreement with both HO-SM and GSM-p. A  $\sim 25\%$  difference between spectroscopic factors in HO-SM and GSM-p is striking. This difference reflects a strong dependence of the two-body matrix elements on the actual radial wave functions. In the GSM-p variant, the g.s. of  ${}^6\text{He}$  is described by an almost pure  $[0p_{3/2} \otimes 0p_{3/2}]^{0+}$  configuration and the resulting spectroscopic factor is close to one in the whole energy region considered. A difference between GSM and GSM-p results illustrates the impact of the non-resonant continuum.

Figures 2-4 display one-neutron radial overlap integrals calculated in GSM for bound  ${}^6\text{He}$  and three energies of the  $0p_{3/2}$  pole corresponding to different physical situations considered in Fig. 1. In Fig. 2, both  ${}^5\text{He}$  and  ${}^6\text{He}$  are bound with one-neutron separation energies 0.5 MeV and 1 MeV, respectively. Figure 3 illustrates the case of unbound  ${}^5\text{He}$  ( $E[{}^5\text{He}] = 0.25 - i0.056$  MeV) and bound  ${}^6\text{He}$  ( $E[{}^6\text{He}] = -0.5$  MeV). Here, the generalized one-neutron separation energy,  $\tilde{S}_{1n}$ , defined as a difference between g.s. binding energies of neighboring nuclei, becomes *complex*:

$$\tilde{S}_{1n}(N) \equiv E(N-1) - E(N) = S_{1n}(N) - \frac{i}{2} [\Gamma(N-1) - \Gamma(N)]. \quad (17)$$

The real part of  $\tilde{S}_{1n}$  is the usual separation energy  $S_{1n}$  while the imaginary

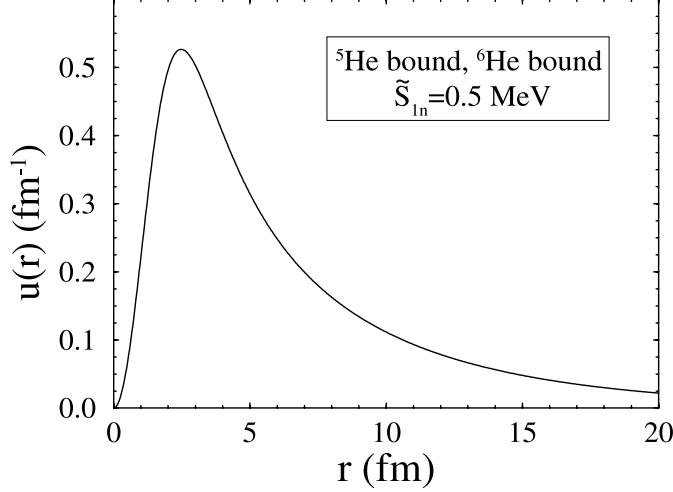


Fig. 2. Single-neutron radial overlap integral  $u(r)$  for the  $\langle {}^6\text{He}(\text{g.s.}) | [{}^5\text{He}(\text{g.s.}) \otimes p_{3/2}]^{0+} \rangle^2$  channel calculated in GSM for one-neutron bound  ${}^5\text{He}$  and  ${}^6\text{He}$ . The radial wave function of the  $0p_{3/2}$  resonant state of the *real* WS potential adjusted to reproduce the GSM value of  $S_{1n}$  in  ${}^6\text{He}$  practically coincides with  $u(r)$ . The overlap integral has been normalized to unity to allow comparison with the WS wave function.

part appears when either parent or daughter nucleus is unbound. Finally, Fig. 4 shows  $u(r)$  for the case of bound  ${}^5\text{He}$  and  ${}^6\text{He}$  having the same energy, i.e.,  $S_{1n}[{}^6\text{He}] = 0$ .

The overlap integral is peaked around the surface ( $\sim 2$  fm) and its asymptotic behavior is determined by one-neutron separation energy [51,52]:

$$u(r) \rightarrow e^{-\kappa r}, \quad (18)$$

where the decay constant is

$$\kappa = \sqrt{2mS_{1n}/\hbar}. \quad (19)$$

In the case considered,  $u(r)$  is expected to decay exponentially with  $\kappa$  determined by the one-neutron separation energy of  ${}^6\text{He}$ . Figures 2-4 show, by the dotted line, the radial wave function of the  $0p_{3/2}$  resonant state of the WS potential with a depth adjusted to reproduce the GSM value of  $S_{1n}$  in  ${}^6\text{He}$ . Since  ${}^6\text{He}$  is one-neutron bound, the corresponding  $0p_{3/2}$  WS state is bound; hence, its wave function is real. It is seen that the agreement between the WS wave function and the real part of  $u(r)$  is excellent.

The situation shown in Fig. 3 is particularly interesting as the overlap integral is complex due to an unbound nature of  ${}^5\text{He}$ . Here, a real WS potential cannot provide any information about the imaginary part of  $u(r)$ . One possible way of

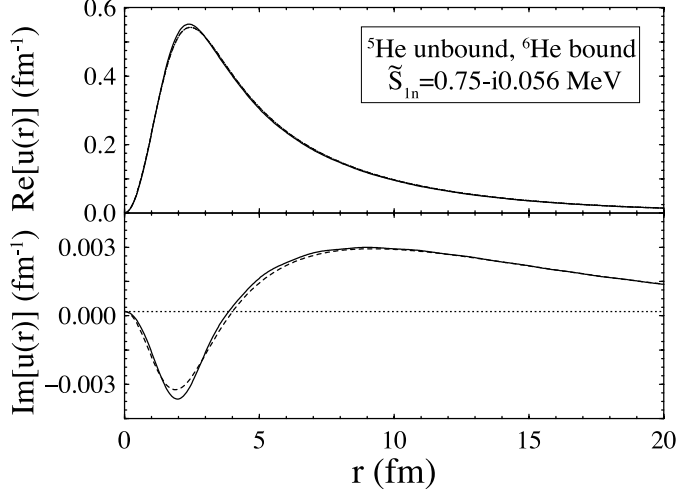


Fig. 3. Solid line: the single-neutron radial overlap integral  $u(r)$  for the  $\langle {}^6\text{He}(\text{g.s.}) | [{}^5\text{He}(\text{g.s.}) \otimes p_{3/2}]^{0+} \rangle^2$  channel calculated in GSM for unbound  ${}^5\text{He}$  and bound  ${}^6\text{He}$ . Dotted line: the radial wave function of the  $0p_{3/2}$  resonant state of the *real* WS potential whose strength was adjusted to reproduce the GSM value of  $S_{1n}$  in  ${}^6\text{He}$ . Dashed line: the radial wave function of the  $0p_{3/2}$  resonant state of the *complex* WS potential whose complex strength was adjusted to reproduce the GSM value of the generalized separation energy  $\tilde{S}_{1n}$  in  ${}^6\text{He}$ . All wave functions are normalized to unity to allow comparison. The real (imaginary) parts of the wave function are shown in the top (bottom) panel.

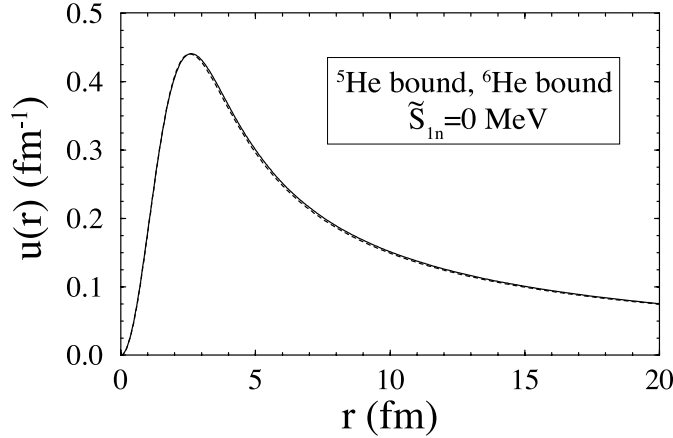


Fig. 4. Similar to Fig. 2 except for the threshold situation of  $S_{1n}[{}^6\text{He}] = 0$ .

overcoming this difficulty is to introduce a *complex* WS potential characterized by a complex strength:

$$V_{WS} \equiv V_{WS}^R + iV_{WS}^I. \quad (20)$$

Following the usual SM strategy applied to real  $u(r)$  cases,  $V_{WS}$  can be adjusted to reproduce the generalized separation energy (17). This guarantees that the asymptotic behavior of the overlap integral, given by Eqs. (18-19) with

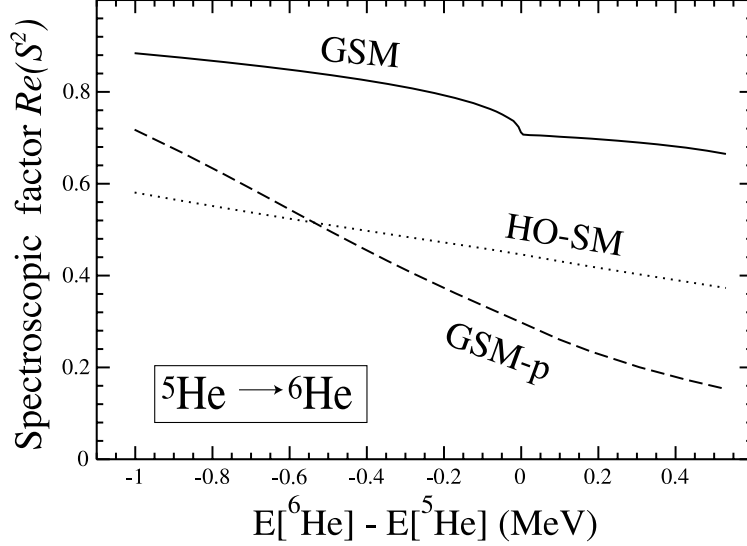


Fig. 5. Similar to Fig. 1 except as a function of (negative)  $S_{1n}$  of  ${}^6\text{He}$ . The depth of the WS potential of  ${}^5\text{He}$  has been adjusted to bind  ${}^5\text{He}$  (see text). The separation energy  $S_{1n}$  of  ${}^6\text{He}$  has been varied by changing the coupling constant  $V_0^{(J=0)}$  of the SGI two-body interaction.

$S_{1n} \rightarrow \tilde{S}_{1n}$ , is correct. (The extension of the discussion of asymptotic properties of  $u(r)$  in Ref. [51] to the complex-energy case is straightforward; it follows from the analytic properties of the vertex form factor.) It is seen in Fig. 3 (dashed line) that both real and imaginary parts of the radial overlap integral are well reproduced by the  $0p_{3/2}$  resonant wave function of a WS potential that reproduces the GSM value of  $\tilde{S}_{1n}$ . This  $0p_{3/2}$  complex-energy state corresponds to a ‘decaying bound state’ which can be found only in the complex s.p. potential (see, e.g., [53,54]); asymptotically, such a state exhibits an exponentially damped oscillation. The effect of the non-resonant continuum is seen in a slightly better localization of the GSM overlap.

Figure 4 illustrates the threshold limit. Here,  $S_{1n}=0$  and  $u(r)$  shows asymptotic behavior that is not exponential. Also in this case the GSM radial overlap integral is well reproduced by the radial  $0p_{3/2}$  WS wave function corresponding to a halo state located at zero energy.

The Wigner estimate for the near-threshold behavior of cross section [35] is independent of the reaction mechanism. While the Wigner limit has been reached in Fig. 1 by changing the pole of the one-body S-matrix, it is interesting to see whether a similar pattern can be generated by many-body correlations. Figure 5 illustrates a direct case of the Wigner cusp. Here, we have fixed the WS potential so that the  $0p_{3/2}$  and  $0p_{1/2}$  shells are both bound with respective energies of  $-5$  MeV and  $-0.255$  MeV, and we have varied the SGI coupling constant  $V_0^{(J=0)}$  so that  $S_{1n}[\text{}^6\text{He}]$  changes sign. The behavior of spectroscopic factor around the  $1n$  threshold is similar to that of Fig. 1, with

the GSM spectroscopic factor exhibiting a non-analytic behavior at  $S_{1n}=0$ . This result constitutes an excellent test of the GSM formalism: the Wigner limit is reached precisely at a threshold obtained from many-body calculations. In the whole range of considered separation energies the HO-SM and GSM-p results vary smoothly and they differ from the GSM results. In this example, the anomalous component of spectroscopic factor is much smaller than the regular component showing the essential role played by the non-resonant continuum component in the ground state of  ${}^6\text{He}$ .

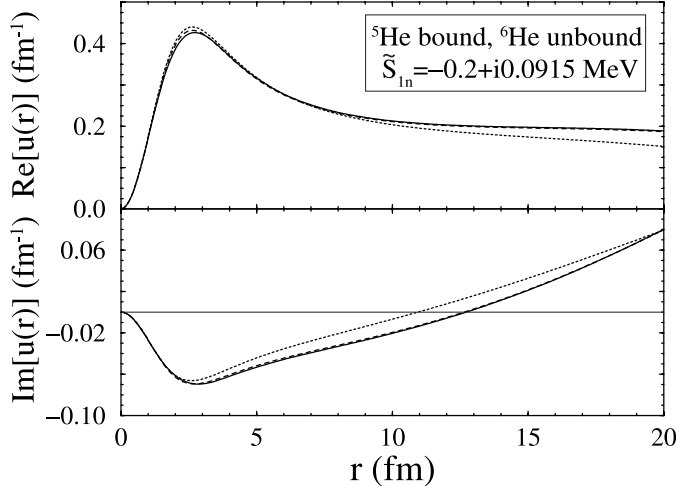


Fig. 6. Similar to Fig. 3 except for bound  ${}^5\text{He}$  and unbound  ${}^6\text{He}$  ( $S_{1n}$  of  ${}^6\text{He}$  is negative.) The dashed line depicts the radial wave function of the  $0p_{3/2}$  resonant state of the complex WS potential whose depth is adjusted to reproduce the GSM value of the generalized separation energy  $\tilde{S}_{1n}$  in  ${}^6\text{He}$ .

Figures 6 and 7 display  $u(r)$  calculated for the two cases shown in Fig. 5 representing unbound  ${}^6\text{He}$ , and  ${}^5\text{He}$  being either bound (Fig. 6) or unbound (Fig. 7). In Fig. 6, the generalized separation energy is complex,  $\tilde{S}_{1n} = -0.2 + i0.0915$  MeV. The corresponding Gamow pole is a bound decaying state. Figure 7 shows the radial overlap integral for unbound  ${}^5\text{He}$  and  ${}^6\text{He}$  having the same real energies, i.e.,  $S_{1n} = 0$ , but different widths. Consequently, the generalized separation energy  $\tilde{S}_{1n}$  has a non-zero imaginary part in this case. The corresponding resonant state lies on the diagonal of the fourth quarter of the complex- $k$  plane.

The radial wave functions of the  $0p_{3/2}$  resonant state of the real WS potential adjusted to the GSM separation energy of  ${}^6\text{He}$  are shown by the dotted lines in Figs. 6 and 7. The agreement between the WS wave function and  $u(r)$  is poor. In particular, their real parts have a different asymptotic behavior. In Fig. 7, the imaginary part of the  $0p_{3/2}$  WS wave function is zero by construction, and it does not reproduce the salient behavior of the imaginary part of  $u(r)$ . On the other hand, the 1n radial overlap integral is very well reproduced by the  $0p_{3/2}$  resonant state wave function of the complex WS potential (dashed curves in Figs. 6, 7).



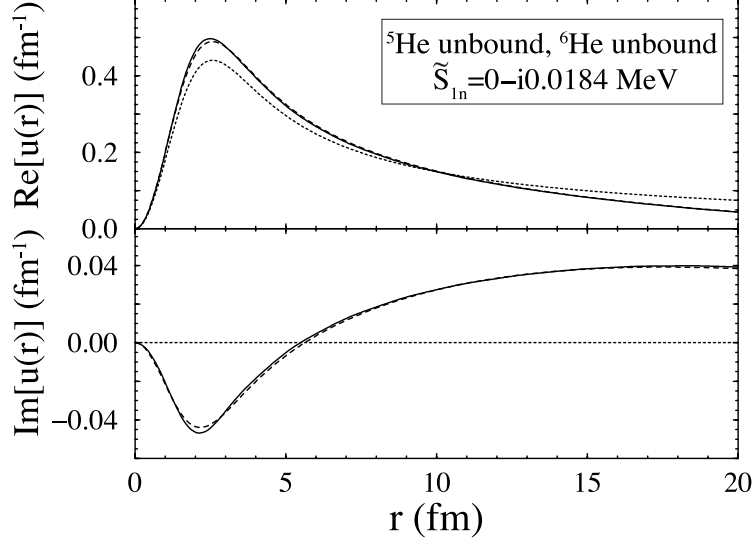


Fig. 7. Similar to Figs. 3 and 6 except for unbound  ${}^5\text{He}$  and  ${}^6\text{He}$ . The  $1n$  separation energy  $S_{1n}$  of  ${}^6\text{He}$  has been adjusted to zero. The generalized  $1n$  separation energy  $\tilde{S}_{1n}$  has a non-vanishing imaginary part.

In general, we find that shapes of  $1n$  overlap integrals calculated in GSM for any complex value of  $\tilde{S}_{1n}$  are well reproduced by radial wave functions of a complex WS potential whose depth is adjusted to reproduce the complex separation energy. In particular, for unbound parent and/or daughter nuclei, the asymptotic behavior of  $u(r)$  is given by the generalized complex separation energy  $\tilde{S}_{1n}$  and not by the real separation energy  $S_{1n}$ .

#### 4.3 The ${}^{17}\text{O}+n \rightarrow {}^{18}\text{O}$ case

To investigate the dependence of spectroscopic factors on the orbital angular momentum  $\ell$  of the transferred nucleon, we consider the  $d_{3/2}$  partial wave in  ${}^{18}\text{O}$ . We show in Fig. 8 the spectroscopic factor for the excited  $0_3^+$  state of  ${}^{18}\text{O}$  in the channel  $[{}^{17}\text{O}(3/2_1^+) \otimes d_{3/2}]^{0^+}$ . The behavior of spectroscopic factor shown in Fig. 8 is similar to that of Fig. 1, except the variations are much weaker (cf. the dramatically expanded scale) and the threshold behavior is different. Namely, the spectroscopic factor is continuous and smooth; it is its derivative that exhibits a cusp around the  $0d_{3/2}$  threshold. Again, this is consistent with the general expectation that, for  $\ell=2$ ,  $Re(S^2)$  below the  $1n$  threshold of  ${}^{17}\text{O}$  behaves as  $(-e_{\ell j})^{3/2}$  while above the threshold  $Re(S^2)$  ( $Im(S^2)$ ) should behave as  $(e_{\ell j})^{3/2}$  ( $(e_{\ell j})^{5/2}$ ). The associated  $1n$   $d_{3/2}$  radial overlap integrals (not displayed) are extremely close to the s.p. resonant  $0d_{3/2}$  wave functions.

To investigate the behavior of spectroscopic factor in  ${}^{18}\text{O}$  around  $S_{1n}=0$ , the depth of the WS potential has been decreased to lower the position of the

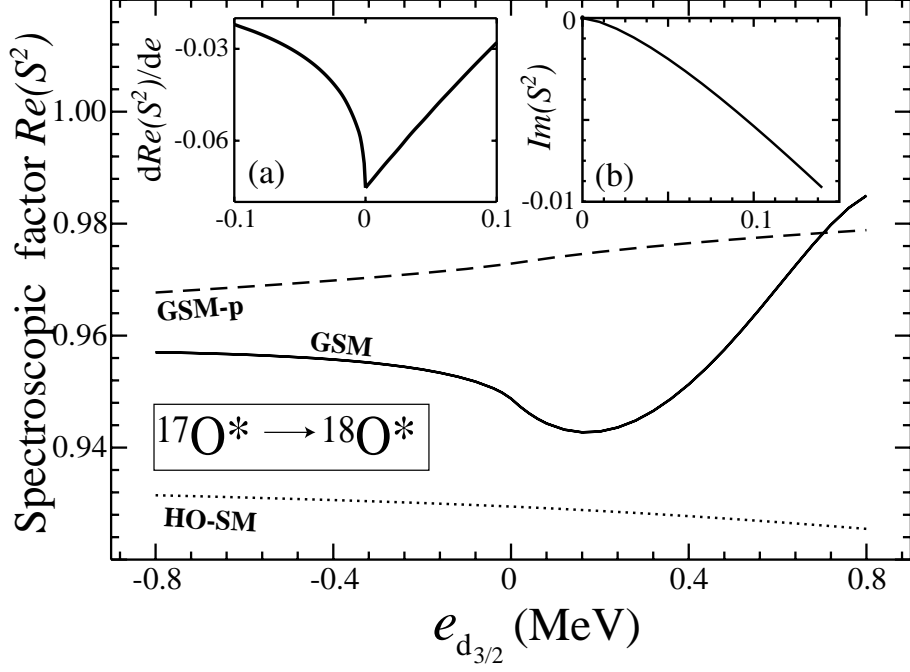


Fig. 8. Similar to Fig. 1 except for the overlap in the excited  $0_3^+$  state of  $^{18}\text{O}$ :  $\langle ^{18}\text{O}(0_3^+) | [^{17}\text{O}(3/2_1^+) \otimes d_{3/2}]^{0^+} \rangle^2$ . The first derivative of the spectroscopic factor in the neighborhood of the  $e_{d_{3/2}}=0$  threshold is shown in the inset (a) while inset (b) displays the imaginary part of  $S^2$ .

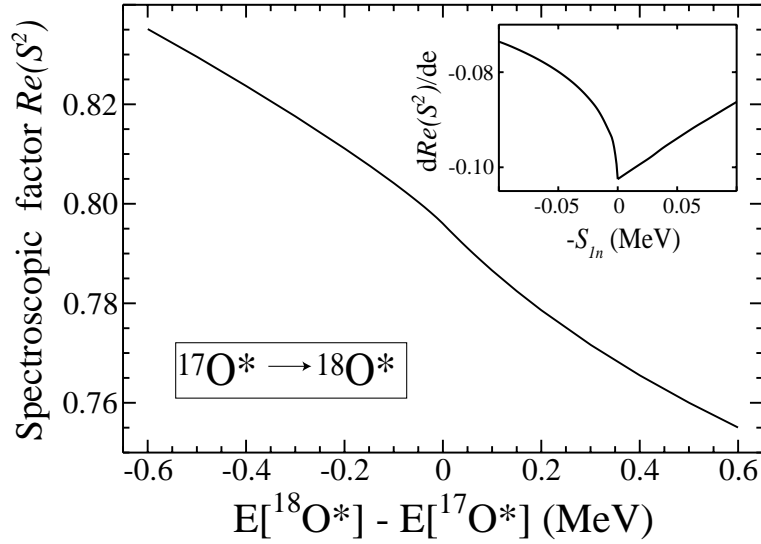


Fig. 9. Similar to Fig. 5 except for the overlap in the excited  $0_3^+$  state of  $^{18}\text{O}$ :  $\langle ^{18}\text{O}(0_3^+) | [^{17}\text{O}(3/2_1^+) \otimes d_{3/2}]^{0^+} \rangle^2$ . The energy derivative of the spectroscopic factor around the  $1n$  threshold is shown in the inset.

$0d_{3/2}$  s.p. pole down to  $-5$  MeV. At the same time, the SDI coupling strength  $V_0$  has been modified to allow  $S_{1n}$  of the  $0_3^+$  state of  $^{18}\text{O}$  to go through zero. The results displayed in Fig. 9 are consistent with the Wigner limit for  $\ell=2$ . Namely, spectroscopic factor and its first derivative are continuous around

$S_{1n}=0$ , while the second derivative exhibits discontinuity (see the inset in Fig. 8). The associated  $1n$   $d_{3/2}$  radial overlap integrals (not displayed) are extremely close to the s.p. resonant  $0d_{3/2}$  wave function of a real (or complex) WS potential.

## 5 Conclusions

By explicit many-body GSM calculations that fully account for a coupling to the scattering space, we demonstrate the presence of a near-threshold, non-perturbative rearrangement in the wave function that has an appreciable low angular momentum s.p. component. The threshold behavior of spectroscopic factors (Wigner cusp) can only be reproduced through a complete inclusion of scattering states, including the non-resonant space, in the GSM basis. Having a complete basis which allows to describe bound, weakly-bound and unbound states on the same footing, is the only way to guarantee the unitarity, which lies at the basis of the Wigner threshold effect in cross sections and other observables, in particular in the multichannel case. This fundamental requirement is not respected in any CQS formulation of the many-body theory. As shown in several examples discussed in our work, restoration of unitarity can strongly affect both values and behavior of spectroscopic factors.

The detailed analysis of near-threshold behavior of spectroscopic factors associated with  $\ell=1$  (heliums) and  $\ell=2$  (oxygens) partial waves shows the presence of the Wigner limit in the many-body GSM solution. Namely, the fluctuating component of the spectroscopic factor behaves as  $(-e_{\ell j})^{\ell-1/2}$  below the  $1n$  threshold. Above the threshold, the spectroscopic factor is complex; the real part behaves as  $(e_{\ell j})^{\ell+1/2}$  while the imaginary part, associated with the decaying nature of a resonance, varies as  $(e_{\ell j})^{\ell-1/2}$ .

If either parent or daughter nucleus is unbound, the corresponding one-nucleon overlap integral is complex. It can be very well approximated by a resonant state of a one-body potential which reproduces the complex generalized one-nucleon separation energy  $\tilde{S}_{1n}$  (17). This is a straightforward generalization of an approximate treatment of one-nucleon overlaps often used in SM studies (see, e.g., Ref. [28]) where a real average potential is employed with a depth adjusted to reproduce  $S_{1n}$ . Therefore, we conclude that the realistic radial overlap functions, which constitute the basic theoretical input needed for a description of transfer reactions, can be conveniently generated by a radial s.p. wave function of the (complex) one-body potential reproducing the generalized separation energy. On the other hand, the normalization of the overlap integral, i.e., the spectroscopic factor, cannot be obtained in a simple way; here the full microscopic treatment is necessary (see discussion in Ref. [10]).

Optimally, the complex average potential used to generate one-nucleon overlap functions should be generated self-consistently using the Gamow-Hartree-Fock procedure [8]. The imaginary part of this potential should not be confused with the absorption potential used in the context of optical model studies. As we illustrated in this paper, depending on  $\tilde{S}_{1n}$ , the corresponding resonant states do not always obey the usual Berggren classification for hermitian Hamiltonians. For instance, one has to consider decaying bound states (resonant states lying in the first quarter of the complex- $k$  plane) or threshold states that have zero energy but nonzero width.

While Berggren never considered complex potentials in the derivation of completeness relation for Gamow states [11,12], its demonstration in the case of localized potentials, as those of the WS type used in this paper, is straightforward [55]. For complex potentials, multiple  $S$ -matrix poles can appear in the resonant-state expansions. This complicates the completeness relation as some additional states, which are not eigenfunctions of the one-body Hamiltonian, have to be added to reach completeness [55]. Moreover, a possible appearance of the spectral singularities, i.e., the  $S$ -matrix poles lying on the real momentum axis, not considered in Ref. [55], can complicate matters [56]. However, multiple singularities cannot happen if the imaginary part of the potential is small enough, and - in this case - the Berggren completeness relation for complex potentials is obtained in the same manner as for real potentials. Such a relation could be useful when developing the generalized Gamow-Hartree-Fock method that deals with unusual Gamow states.

This work was supported by the U.S. Department of Energy under Contracts Nos. DE-FG02-96ER40963 (University of Tennessee), DE-AC05-00OR22725 with UT-Battelle, LLC (Oak Ridge National Laboratory), and DE-FG05-87ER40361 (Joint Institute for Heavy Ion Research).

## References

- [1] J. Dobaczewski, and W. Nazarewicz, *Phil. Trans. R. Soc. Lond. A* **356** (1998) 2007.
- [2] B.A. Brown, *Prog. Part. Nucl. Phys.* **47** (2001) 517.
- [3] J. Okołowicz, M. Płoszajczak, and I. Rotter, *Phys. Rep.* **374** (2003) 271.
- [4] E. Caurier, G. Martnez-Pinedo, F. Nowacki, A. Poves, and A.P. Zuker, *Rev. Mod. Phys.* **77** (2005) 427.

- [5] R.G. Thomas, Phys. Rev. **81** (1951) 148;  
R.G. Thomas, **88** (1952) 1109;  
J.B. Ehrman, Phys. Rev. **81** (1951) 412.
- [6] J. Dobaczewski, N. Michel, W. Nazarewicz, M. Płoszajczak, and J. Rotureau, Prog. Part. Nucl. Phys. **59** (2007) 432.
- [7] N. Michel, W. Nazarewicz, M. Płoszajczak, and K. Bennaceur, Phys. Rev. Lett. **89** (2002) 042502;  
N. Michel, W. Nazarewicz, M. Płoszajczak, and J. Okołowicz, Phys. Rev. C **67** (2003) 054311.
- [8] N. Michel, W. Nazarewicz, and M. Płoszajczak, Phys. Rev. C **70** (2004) 064313.
- [9] R.I. Betan, R.J. Liotta, N. Sandulescu, and T. Vertse, Phys. Rev. Lett. **89** (2002) 042501;  
R.I. Betan, R.J. Liotta, N. Sandulescu, and T. Vertse, Phys. Rev. C **67** (2003) 014322.
- [10] N. Michel, W. Nazarewicz, and M. Płoszajczak, Phys. Rev. C **75** (2007) 031301(R).
- [11] T. Berggren, Nucl. Phys. A **109** (1968) 265.
- [12] T. Berggren and P. Lind, Phys. Rev. C **47** (1993) 768.
- [13] I. Gelfand and N. Ya. Vilenkin, *Generalized Functions*, Volume 4, (Academic Press, New York 1964).
- [14] A. Bohm, *The Rigged Hilbert Space and Quantum Mechanics*, Lecture Notes in Physics **78** (Springer, New York 1978).
- [15] R. de la Madrid, Eur. J. Phys. **26** (2005) 287.
- [16] O. Civitarese and M. Gadella, Phys. Rep. **396** (2004) 41.
- [17] G. Hagen and J. Vaagen, Phys. Rev. C **73** (2006) 034321.
- [18] R. Freund, Lanczos Method for Complex Symmetric Eigenproblems (Section 7.11), in Z. Bai, J. Demmel, J. Dongarra, A. Ruhe, and H. van der Vorst, editors, *Templates for the Solution of Algebraic Eigenvalue Problems: A Practical Guide*, SIAM, Philadelphia, 2000.
- [19] S.R. White, Phys. Rev. Lett. **69** (1992) 2363; S.R. White, Phys. Rev. B **48** (1993) 10345.
- [20] J. Rotureau, N. Michel, W. Nazarewicz, M. Płoszajczak, and J. Dukelsky, Phys. Rev. Lett. **97** (2006) 110603.
- [21] O. Civitarese, M. Gadella, and R. Id Betan, Nucl. Phys. A **660** (1999) 255.
- [22] G.R. Satchler, *Direct Nuclear Reactions* (Clarendon Press, Oxford, 1983).
- [23] M.H. Macfarlane and J.B. French, Rev. Mod. Phys. **32** (1960) 567.

- [24] N.K. Glendenning, *Ann. Rev. Nucl. Sci.* **13** (1963) 191;  
N.K. Glendenning, *Direct Nuclear Reactions* (Academic Press Inc., 1983).
- [25] P. Fröbrich and R. Lipperheide, *Theory of Nuclear Reactions* (Oxford Science Publications, Clarendon Press Oxford, 1996)
- [26] Jenny Lee *et al.*, arXiv:nucl-ex/0511023;  
M.B. Tsang, Jenny Lee, and W. G. Lynch, *Phys. Rev. Lett.* **95** (2005) 222501.
- [27] P.G. Hansen and J.A. Tostevin, *Ann. Rev. Nucl. Part. Sci.* **53** (2003) 219.
- [28] A. Gade *et al.*, *Eur. Phys. J. A* **25** (2005) s01, 251;  
D. Bazin *et al.*, *Phys. Rev. Lett.* **91** (2003) 012501.
- [29] A.M. Mukhamedzhanov and F.M. Nunes, *Phys. Rev. C* **72** (2005) 017602.
- [30] R.J. Furnstahl and H.-W. Hammer, *Phys.Lett. B* **531** (2002) 203.
- [31] J.A. Tostevin, *J. Phys. G: Nucl. Part. Phys.* **25** (1999) 735;  
V. Maddalena *et al.*, *Phys. Rev. C* **63** (2001) 024613;  
B.A. Brown, P.G. Hansen, B.M. Sherrill, and J.A. Tostevin, *Phys. Rev. C* **65** (2002) 061601.
- [32] A. Bohr and B.R. Mottelson, *Nuclear Structure*, Vol. 1 (New York, W.A. Benjamin, 1969).
- [33] B. Gyarmati, F. Krisztinkovics and T. Vertse, *Phys. Lett. B* **41** (1972) 110.
- [34] T. Berggren, *Phys. Lett. B* **373** (1996) 1.
- [35] E.P. Wigner, *Phys. Rev.* **73** (1948) 1002.
- [36] C. Hategan, *Annals of Physics* **116** (1978) 77.
- [37] G. Graw and C. Hategan, *Phys. Lett. B* **37** (1971) 41.
- [38] J. Okołowicz and M. Płoszajczak, *Int. J. Mod. Phys. E* **15** (2006) 529;  
Y. Luo, J. Okolowicz, M. Ploszajczak, and N. Michel, arXiv:nucl-th/0211068.
- [39] G. Breit, *Phys. Rev.* **107** (1957) 1612.
- [40] A.I. Baz, *Soviet Phys. - JETP* **6** (1957) 709.
- [41] R.G. Newton, *Phys. Rev.* **114** (1959) 1611.
- [42] W.E. Meyerhof, *Phys. Rev.* **129** (1963) 692.
- [43] A.I. Baz, Y.B. Zeldovich, and A.M. Peremolov, *Scattering, Reactions and Decays in Nonrelativistic Quantum Mechanics*, (Jerusalem, 1969, translated from Russian, Nauka, Moscow, 1966).
- [44] A.M. Lane, *Phys. Lett. B* **33** (1970) 274.
- [45] C. Hategan, *Proc. Rom. Acad. A* **3** (2002) 11.
- [46] P.R. Malmberg, *Phys. Rev.* **101** (1956) 114.

- [47] J.T. Wells, A.B. Tucker, and W.E. Meyerhof, Phys. Rev. **131** (1963) 1644.
- [48] C.F. Moore *et al.*, Phys. Rev. Lett. **17** (1966) 926.
- [49] S. Abramovich, B. Guzhovskij, and L. Lasarev, Sov. J. Part. Nucl. **23** (1992) 129.
- [50] W.H. Dickhoff and C. Barbieri, Prog. Part. Nucl. Phys. **52** (2004) 377.
- [51] L.D. Blokhintsev, I. Borbely, and E.I. Dolinskii, Sov. J. Part. Nucl. **8** (1977)c485.
- [52] N.K. Timofeyuk, L.D. Blokhintsev, and J.A. Tostevin, Phys. Rev. C **68** (2003) 021601(R).
- [53] D. Baye, G. Levai, and J.-M. Sparenberg, Nucl. Phys. A **599** (1996) 435.
- [54] V.M. Chabanov and B.N. Zakhariev, Inverse Problems **17** (2001) 683.
- [55] M.V. Nikolayev and V.S. Olkhovsky, Lett. Nuo. Cime. **8** (1973) 703.
- [56] B.F. Samsonov, J. Phys. A: Math. Gen. **38** (2005) L571.